Post-print of: Puchalski B., Rutkowski T., Duzinkiewicz K.: Nodal models of Pressurized Water Reactor core for control purposes – A comparison study. NUCLEAR ENGINEERING AND DESIGN. Vol. 322 (2017), pp. 444-463. DOI: 10.1016/j.nucengdes.2017.07.005

Nodal models of Pressurized Water Reactor core for control purposes – a comparison study

Bartosz Puchalski*, Tomasz A. Rutkowski*, Kazimierz Duzinkiewicz*

Department of Control Systems Engineering, Faculty of Electrical and Control Engineering, Gdansk University of Technology, G. Narutowicza Street 11/12, 80-233 Gdansk, Poland

Abstract

The paper focuses on the presentation and comparison of basic nodal and expanded multi-nodal models of the Pressurized Water Reactor (PWR) core, which includes neutron kinetics, heat transfer between fuel and coolant, and internal and external reactivity feedback processes. In the expanded multi-nodal model, the authors introduce a novel approach to the implementation of thermal power distribution phenomena into the multi-node model of reactor core. This implementation has the form of thermal power distribution coefficients which approximate the thermal power generation profile in the reactor. It is assumed in the model that the thermal power distribution is proportional to the axial distribution of neutron flux in the un-rodded and rodded reactor core regions, as a result of control rod bank movements. In the paper, the authors propose a methodology to calculate those power distribution coefficients, which bases on numerical solutions of the transformed diffusion equations for the un-rodded and rodded reactor regions, respectively. Introducing power distribution coefficients into the expanded multi-nodal model allows to achieve advanced capabilities that can be efficiently used in design and synthesis of more advanced and complex control algorithms for PWR reactor core, for instance in the field of reactor temperature distribution control.

*Corresponding author

Email addresses: bartosz.puchalski@pg.edu.pl (Bartosz Puchalski), tomasz.adam.rutkowki@pg.edu.pl (Tomasz A. Rutkowski), kazimierz.duzinkiewicz@pg.edu.pl (Kazimierz Duzinkiewicz)

Keywords: Modelling, Nodal model, Pressurized Water Reactor, Flux shape, Power distribution

1. Introduction

The mathematical models of nuclear reactor processes can be divided into two main groups, the first of which is related to complex and accurate models, while the second represents less accurate, reduced and simple models. These two groups have different applications and purposes. The first group models may be used in design of reactor core, safety considerations, or detailed analyses of phenomena and nature of processes occurring in the nuclear reactor core. On the other hand, the less accurate models composing the second group can be used in control systems synthesis, and for education or training purposes. The second group models should also comply with several aspects which the first group is unable to fulfil, for instance easy implementation, convenient calculation time, or simple description. This paper focuses on the second group of models, with emphasis on nuclear reactor control systems and algorithm synthesis.

Several approaches can be efficiently used in that field, of which the lumped parameter models are most common and widely utilized. In (Han, 2000) the author presents dynamic models for the primary loop systems of nuclear power plants, which have the potential of fast running on personal computers. These models have been mainly made for thermal-hydraulic analysis purposes. Another example is the paper (Fazekas et al., 2007), in which the authors present simplified dynamic models of primary circuit elements of a nuclear power plant for control system design purposes. Also in (Dong et al., 2009) the authors present lumped parameter dynamic models of primary loop elements for control system design and simulation, while in (Karla et al., 2015; Tarnawski and Karla, 2016) the authors present an approach to building lumped model based low cost non-real-time and real-time nuclear reactor simulators. Lumped parameter models can also be utilized in advanced process control. Authors in (Kulkowski et al., 2015; Sokolski et al., 2016) presents simple and complex non-linear dy-

namic models of nuclear power plant steam turbine used for that purposes.

Another modelling approach is the usage of fractional calculus. In (Espinosa-Paredes et al., 2011; Nowak et al., 2014a,b) the authors present similar ways of modelling neutron point kinetics equations which play a significant role in the reduced models of nuclear reactor core. Also in (Nowak et al., 2015) the authors introduce fractional order neutron kinetics equations, along with the integer order heat transfer model. The fractional order models are more complex than the lumped non-fractional parameter models, because of more sophisticated computational methods to be applied. On the other hand, they have an ability to mimic some physical processes in a more accurate way.

The last, but not least, field in simplified modelling of nuclear processes is nodal approach. Nodal methods divide the distributed systems into smaller parts (nodes) which can be modelled by ordinary differential equations. Due to a high number of computational nodes used, these models are most complex, yet still capable of performing calculations in convenient time. The nodal models are also interesting for their ability to model spatial relations in the modelled elements with little effort. The point kinetics approach is not proper in some types of nuclear reactors, as stated in (Dong et al., 2010). The authors of that paper derive the nodal neutron kinetics model with corresponding nodal thermal-hydraulic models of nuclear reactor core. In (Puchalski et al., 2016) the authors derive nodal thermal-hydraulic models of reactor core with corresponding power distribution coefficients, while in (Sharma et al., 2003; Tiwari et al., 1996), for control purposes of xenon induced spatial oscillations, the authors divide the nodal model of reactor core into a number of zones, which are then treated as small cores coupled through neutron diffusion – a concept of coupled-core kinetics.

In (Zhang, 2012; Zhang and E. Holbert, 2013) the authors compare nodal and distributed parameter models in the frequency domain and identify advantages and disadvantages of each model, while in (Puchalski et al., 2015a; Guimarães et al., 2008) the authors present simple and multi-nodal models of the U-tube steam generator, a crucial element in the nuclear power plant, for control and

simulation purposes. For example, in (Puchalski et al., 2015a) and (Puchalski et al., 2015b) the multi-regional fuzzy controller, with local PID controllers and Takagi-Sugeno reasoning mechanism for U-tube steam generator water level control, and the membership functions tuning procedure is described.

The nodal models presented in the paper are based on the point kinetics model to describe the time-depended average neutron population including the delayed neutrons in the reactor core. Moreover, they make use of a nodal approach to describe the heat transfer between the reactor fuel and coolant, and the reactivity feedback influences related to the main internal and external mechanism of fuel and coolant temperature changes and control rod bank movement. In the paper the authors expand the nodal approach presented mainly in (Kerlin, 1978) and applied in (Naghedolfeizi, 1990; Kapernick, 2015; Liu, 2015; Perillo, 2010) by adding special thermal power distribution coefficients to approximate thermal power generation distribution in the reactor core with respect to the reactor control rod bank movement.

This paper is organized as follows. In Section 2 the point kinetics model is briefly described, while in Section 3 basic nodal models of the PWR reactor core are described and compared in simulation. In Section 4 the extended multi-nodal model of PWR reactor core is described in detail, including: model equations, different cases of thermal power distribution coefficient calculations, comparison of simulation results for selected number of fuel nodes, and comparison with dedicated nuclear simulation and analysis software. Finally, conclusions are presented in Section 5.

2. Point kinetics model of the reactor core

In general, the behaviour of the distributed physical systems can be represented by lumped point models. Partial differential equations, commonly used to describe spatial systems, can be simplified to ordinary differential equations with a finite number of parameters. With this simplification, the space dependent nature of the process can be neglected by using averaged physical quan-

tities. For the nuclear reactor core, the point model describes average values of the neutron density and the temperature of fuel or coolant, i.e. the physical quantities which are most important for reactor core operation.

In the paper, the point kinetics model of nuclear reactor core is used to describe the time-depended average neutron population, including six groups of delayed neutrons. It is featured by a well-known set of ordinary differential equations Duderstadt and Hamilton (1976).

$$\frac{d\bar{n}(t)}{dt} = \frac{\rho(t) - \beta}{\Lambda}\bar{n}(t) + \sum_{i=1}^{6} \lambda_i C_i(t), \tag{1}$$

$$\frac{dC_i(t)}{dt} = \frac{\beta_i}{\Lambda}\bar{n}(t) - \lambda_i C_i(t), \quad i = 1, ..., 6, \tag{2}$$

where $\bar{n}$ is the average neutron density, ρ is the reactivity, $\beta = \sum_{i=1}^{6} \beta_i$ is the total yield of the delayed neutron precursors, Λ is the average neutron generation time, λ_i are the decay constants of the delayed neutron precursors, C_i are the concentrations of the i-th group of the delayed neutron precursors, β_i are yields of the delayed neutron precursors, and t is the time.

Taking into account the well-known fact that the thermal power generated in the reactor core is proportional to the neutron flux and the average neutron density

$$P_{TH}(t) \sim \phi \sim \bar{n}, \tag{3}$$

the thermal power generated in the reactor core is assumed to be calculated from the formula

$$P_{TH}(t) = \frac{\bar{n}(t)}{N_{0,N}} P_{TH,N}, \tag{4}$$

where P_{TH} is the reactor thermal power, $N_{0,N}$ is the nominal average neutron density at full power, $P_{TH,N}$ is the nominal power of the reactor core, and ϕ denotes the neutron flux. The values of numerical parameters of the PWR reactor point kinetic model are included in Appendix A. The heat transfer processes, and the reactivity feedback due to the fuel temperature, coolant temperature, and control rod bank movements, are also taken into account and described in detail in the following sections for the appropriate reactor nodal models.

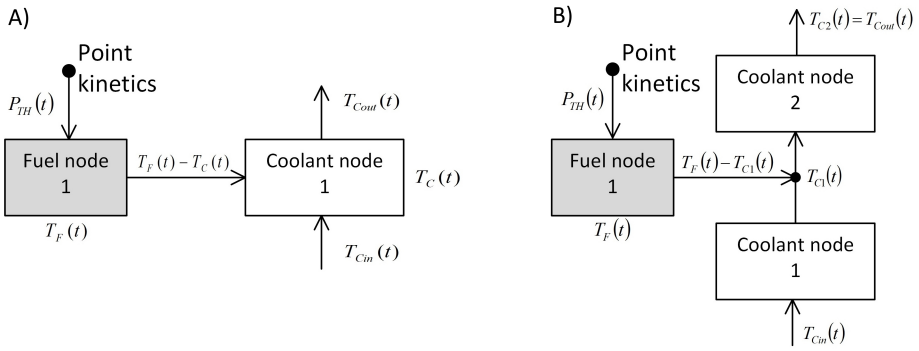

Figure 1: Basic heat transfer nodal models of nuclear reactor core: A) with one fuel node and one coolant node (1F/1C); B) with one fuel node and two coolant nodes (1F/2C).

3. Basic heat transfer nodal models of the reactor core

This section focuses on two basic nodal models of heat transfer in the reactor core, Fig. 1. These models are most popular and widely used in the field of control algorithm synthesis. The first nodal model includes one fuel node and one coolant node – 1F/1C (Fig. 1A), while the second model has the structure with one fuel and two coolant nodes, respectively – 1F/2C (Fig. 1B). In both cases, the heat generated at the fuel node is calculated using the point kinetics model described in the previous section. The coolant nodes are treated as well-stirred tanks (Kerlin, 1978). Also, the heat transfer between the fuel node and the coolant node is proportional to the differences between the temperature of the fuel node and the temperature of the coolant in the coolant node (Fig. 1A)) or the temperature of the coolant on the outlet of the first coolant node, same as in the inlet to the second coolant node (Fig. 1B)).

3.1. The nodal model 1F/1C

The mathematical model of heat balance between one fuel and one coolant node (Fig. 1A) is derived from the classic Newton law of cooling and is described by two differential equations

$$m_F c_{pF} \frac{dT_F(t)}{dt} = f_F P_{TH}(t) - Ah(T_F(t) - T_C(t)), \tag{5}$$

$$m_C c_{pC} \frac{dT_C(t)}{dt} = (1 - f_F) P_{TH}(t) + Ah(T_F(t) - T_C(t)) + \\ - W_C c_{pC}(T_{Cout}(t) - T_{Cin}), \tag{6}$$

where m_F is the mass of the fuel, c_{pF} is the specific heat capacity of the fuel, T_F is the fuel temperature, f_F is the fraction of the total power generated in the fuel, A the is effective heat transfer area, h is the average overall heat transfer coefficient, T_C is the average coolant temperature, m_C is the mass of the coolant, c_{pC} is the specific heat capacity of the coolant, W_C is the coolant mass flow rate within the core, T_{Cout} is the coolant outlet temperature, and T_{Cin} is the coolant inlet temperature.

In accordance with the assumed heat balance model (5)-(6), the average coolant temperature at the coolant node is determined as the mean value of the inlet and outlet coolant temperatures

$$T_C(t) = \frac{T_{Cout}(t) + T_{Cin}(t)}{2}. \tag{7}$$

Finally, after rearranging Equation (7) the outlet coolant temperature can be expressed as

$$T_{Cout}(t) = 2T_C(t) - T_{Cin}(t), \tag{8}$$

while the reactivity feedback balance related to the main internal mechanisms (fuel and coolant temperature effects) and external mechanisms (control rod bank movements) for this model can be represented by the algebraic equation

$$\rho(t) = \rho_{ext} + \alpha_F(T_F(t) - T_{F,0}) + \alpha_C(T_C(t) - T_{C,0}), \tag{9}$$

where ρ_{ext} is the deviation of the external reactivity from the initial (critical) value, α_F is the fuel reactivity coefficient, $T_{F,0}$ is the initial condition for the fuel temperature, α_C is the coolant reactivity coefficient, $T_{C,0}$ is the initial condition for the average coolant temperature.

Unfortunately, the above presented point model has a main drawback resulting from the use of Equation (8). When a sudden increase/decrease in the inlet coolant temperature takes place, the temperature of the outlet coolant will

instantly decrease/increase at the same time. This effect is incorrect and does not agree with the reality. The values of the numerical parameters in the nodal model 1F/1C are included in Appendix A.

3.2. The nodal model 1F/2C

The nodal model 1F/2C has the structure consisting of one fuel and two coolant nodes – Mann's model (Fig. 1B). In that model, the driving temperature difference is changed into the temperature difference between the fuel and the average temperature of the first coolant node. Hence, an assumption is made that the temperature of the coolant on the outlet of the considered coolant node equals the average coolant temperature in the considered coolant node. In that case, the mathematical model of heat balance between nodes is composed of three ordinary differential equations (Kerlin, 1978; Kapernick, 2015; Liu, 2015; Perillo, 2010).

The first equation describes the heat balance for the fuel node

$$m_F c_{pF} \frac{dT_F(t)}{dt} = f_F P_{TH}(t) - Ah(T_F(t) - T_{C1}(t)), \tag{10}$$

where T_{C1} is the average coolant temperature in the first coolant node.This equation is similar to Equation (5) due to the presence of one fuel node, as shown in Fig. 1A.

The second and third differential equation describe heat balances for first and second coolant nodes of 1F/2C model (Fig. 1B) as follows

$$\begin{aligned} \frac{m_C}{2} c_{pC} \frac{dT_{C1}(t)}{dt} = (1 - f_F)\frac{P_{TH}(t)}{2} + \frac{A}{2}h(T_F(t) - T_{C1}(t)) + \\ - W_C c_{pC}(T_{C1}(t) - T_{Cin}(t)), \end{aligned} \tag{11}$$

$$\begin{aligned} \frac{m_C}{2} c_{pC} \frac{dT_{C2}(t)}{dt} = (1 - f_F)\frac{P_{TH}(t)}{2} + \frac{A}{2}h(T_F(t) - T_{C1}(t)) + \\ - W_C c_{pC}(T_{C2}(t) - T_{C1}(t)), \end{aligned} \tag{12}$$

where T_{C2} is the average coolant temperature at the second node, also considered as the coolant outlet temperature.

The reactivity feedback balance for the nodal model 1F/2C takes the form of the following algebraic equation

$$\rho(t) = \rho_{ext} + \alpha_F(T_F(t) - T_{F,0}) + \frac{\alpha_C}{2}(T_{C1}(t) - T_{C1,0}) + \\ + \frac{\alpha_C}{2}(T_{C2}(t) - T_{C2,0}). \tag{13}$$

Due to two coolant nodes considered in the nodal model 1F/2C, some variables and parameters in Equations (11)-(13) are divided by 2.

The main advantage of this model results from a more realistic description of heat transfer from fuel to coolant, compared to the model with one coolant node which assumes that the average coolant temperature in the coolant node is the mean value of its inlet and outlet coolant temperatures. This approach prevents unnatural static temperature changes at the coolant output node.

3.3. Comparison of simulation results for nodal models 1F/1C and 1F/2C

This subsection compares two basics nodal models, namely 1F/1C and 1F/2C (Fig. 1). It is shown how the introduction of two coolant nodes affects the average neutron density $\frac{n}{n_0}$ related to the thermal power P_{TH} of the reactor core, the temperatures T_F at the fuel node and T_C at the coolant nodes, and the outlet coolant temperature T_{Cout}.

Figure 2 shows the responses of the reactor core nodal models to the negative step change of reactivity $\Delta\rho$ (control rod bank insertion into the reactor core), made at the fifth second of simulation, with the final value equal to -5 cents, while Fig. 3 illustrates the model responses to the negative step change of coolant inlet temperature ΔT_{Cin}, with the final value equal to -5% of the nominal value. Finally, the responses to the negative step change of coolant mass flow rate ΔW_C is shown in Fig. 4, and its final value is equal to -3% of the nominal coolant mass flow through the reactor core.

In all Figs. 2-4 minor differences in relative values of all presented variables can be seen, while comparing their dynamic behaviour indicates that all waveforms have a similar character. The Fig. 2 shows that the temperatures calculated at both fuel and coolant nodes by the 1F/1C model are lower than those

calculated by the 1F/2C model. Moreover, the average neutron density calculated by the 1F/1C model is also lower than that calculated by the 1F/2C model. Intuitively, the average neutron density results are expected to be reversed for that two types of models. However, the sum of fuel and coolant reactivity feedbacks, calculated for each model from Equation (9) and (13) respectively, shows that the reactivity from internal feedbacks obtained for the 1F/2C model is slightly higher in value than that for the 1F/1C model. This fact directly explains the reverse trend in average neutron density changes. Major differences between the models can be seen especially in the coolant temperature at reactor outlet, presented in Fig. 3, where the negative step change of the coolant inlet temperature is introduced. In that case, the coolant outlet temperature calculated from the nodal model with only one coolant node (1F/1C) changes statically to 325.8 $°C$ at the fifth second of simulation. This change is caused by the method of coolant outlet temperature calculation that is related to the formula presented by Equation (8). From this formula, it can be concluded that

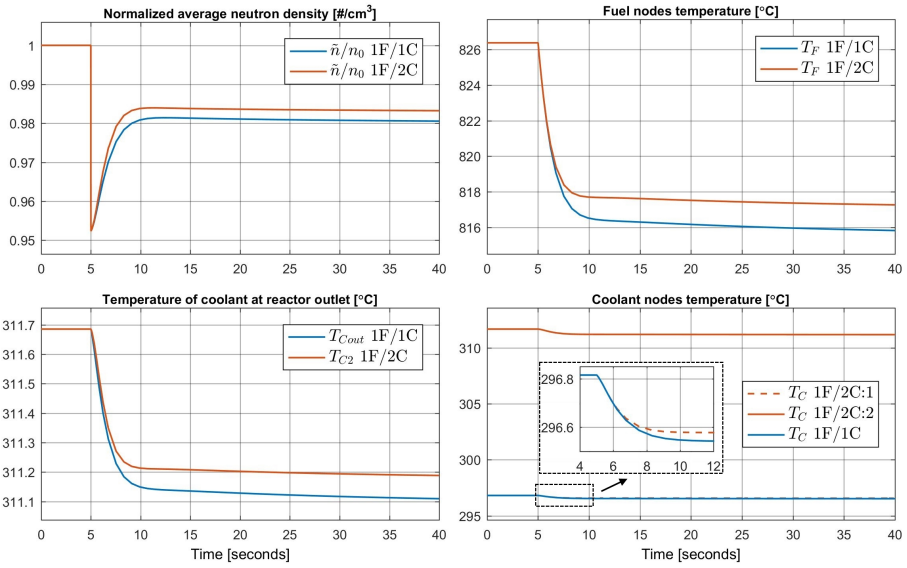

Figure 2: Comparison of models with one fuel node – negative external reactivity step change $\Delta\rho = -5c$ (control rod bank insertion into reactor core).

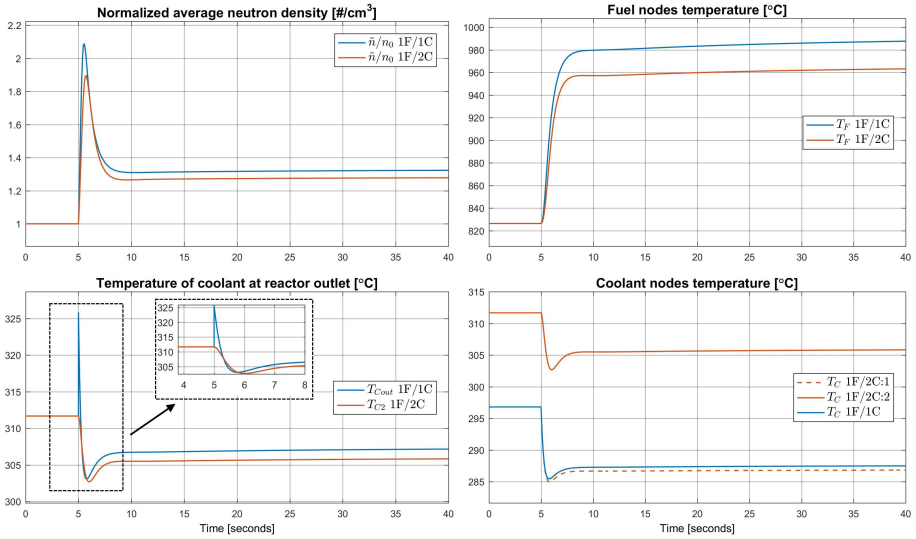

Figure 3: Comparison of models with one fuel node – negative coolant inlet temperature step change $\Delta T_{Cin} = -5\%$.

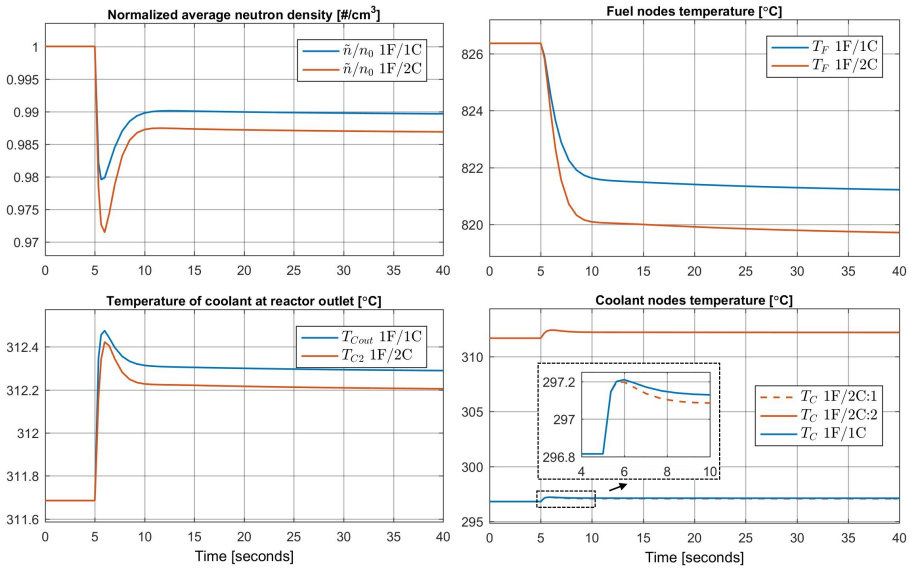

Figure 4: Comparison of models with one fuel node – negative mass flow rate step change $\Delta W_C = -3\%$.

each change of coolant inlet temperature will be immediately followed by an instant change of coolant outlet temperature. This effect is invalid and undesirable, as it affects the negative reactivity feedback. Hence, the1F/1C model is inappropriate for that specific control purposes. On the other hand, the nodal model with two coolant nodes (1F/2C) lacks this disadvantage, due to introducing the second coolant node to the heat transfer structure of the model. Let us note that the temperature of the second coolant node is treated as the coolant outlet temperature from the reactor core (Fig. 1B).

4. Expanded heat transfer multi-nodal model of the reactor core

The concept of the expanded multi-nodal reactor core model is shown in Fig. 5. This approach is an expansion of the previously described basic nodal model of heat transfer (subsection 3.2). It may be treated as discrete approximation of the spatial model. By adding more fuel and coolant nodes the multi-nodal model is getting closer to the spatial model, yet still preserving simple mathematical description.

The alteration of thermal power distribution in the reactor core is mainly caused by control rod bank movement and/or poisoning or depletion of the nuclear fuel, and has direct impact on the fuel and coolant temperatures in particular zones of the reactor core. In the paper the authors introduce power distribution phenomena to the multi-node model in the form of power distribution coefficients D_{Ci}, which approximate the thermal power generated in all nodes of the multi-nodal model of the operating reactor, with special emphasis on the control rod bank movement. In the simplest case, those coefficients may be equal and constant over time and over the space of the reactor core (subsection 4.2.1) – uniform power generation profile. Alternatively, they can be kept constant in time, but related to the nominal axial distribution of the neutron flux along the reactor core height (subsection 4.2.2). In those cases, only the information about the unchanged (nominal) shape of the neutron flux is used to calculate the power distribution coefficients D_{Ci}. This insensibility of

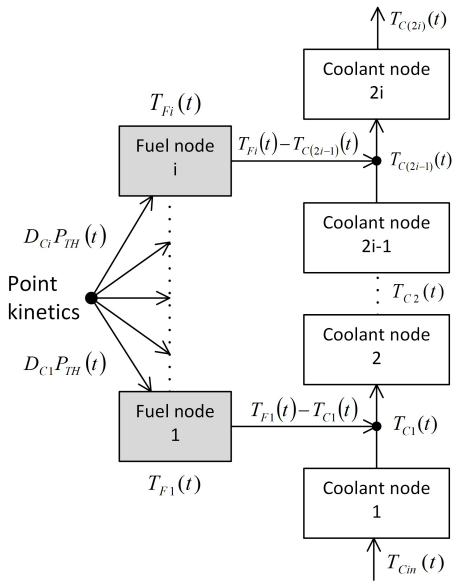

Figure 5: Expanded heat transfer multi-nodal reactor model.

the neutron flux to the control rod bank movement can be observed in tightly coupled cores, in which the reactor core height/migration length (H/M) ratio is small and ranges from a few to slightly more than ten (Lewis, 2008). For loosely coupled cores, in which the values of the H/M ratio can reach several dozens, strong deviations of axial neutron flux distribution are observed (Lewis, 2008). In those cases, the power distribution coefficients D_{Ci} should be treated as variable parameters which depend on time and reactor region changes resulting from the control rod bank movement – insertion to the depth x from the top of the reactor. This case is represented by power distribution coefficients of Type III (subsection 4.2.3). The parameters of the PWR reactor core analysed in the paper give the value of the H/M ratio equal to 48.

4.1. Mathematical model

The heat balance equations for the $i-$th fuel/coolant node of the expanded multi-nodal model of reactor core (Fig.5), can be presented as follows

$$\frac{dT_{Fi}(t)}{dt} = \frac{\eta f_F P_{TH}(t) D_{Ci}}{m_F c_{pF}} - \frac{Ah}{m_F c_{pF}}(T_{Fi}(t) - T_{C(2i-1)}(t)), \tag{14}$$

$$\frac{dT_{C(2i-1)}(t)}{dt} = \frac{2\eta(1-f_F)P_{TH}(t)\frac{D_{Ci}}{2}}{m_C c_p C} + \frac{Ah}{m_C c_{pC}}(T_{Fi}(t) - T_{C(2i-1)}(t)) + \\ - \frac{2nW_C}{m_C}(T_{C(2i-1)}(t) - T_{C(2i-2)}(t)), \tag{15}$$

$$\frac{dT_{C(2i)}(t)}{dt} = \frac{2\eta(1-f_F)P_{TH}(t)\frac{D_{Ci}}{2}}{m_C c_p C} + \frac{Ah}{m_C c_{pC}}(T_{Fi}(t) - T_{C(2i-1)}(t)) + \\ - \frac{2nW_C}{m_C}(T_{C(2i)}(t) - T_{C(2i-1)}(t)), \tag{16}$$

where η denotes the number of fuel nodes, D_{Ci} are the thermal power distribution coefficients, which for instance may depend on the depth x of control bank immersion into the reactor core, $i = 1, ..., \eta$ represents the fuel node index, $2i-1$ is the odd coolant node index and $2i$ is the even coolant node index. It should be noted that temperature T_{C0} which results from substitution of $i = 1$ to equation (15) is related to inlet coolant temperature $T_{C,in}$.

The reactivity feedback balance for the expanded multi-nodal model (Equations (14)-(16)) is described as

$$\rho(t) = \rho_{ext} + \alpha_F \sum_{i=1}^{\eta}[D_{Ci} \cdot (T_{Fi}(t) - T_{Fi,0})] + \\ + \alpha_C \sum_{i=1}^{\eta}[\frac{1}{2}D_{Ci} \cdot (T_{C(2i-1)}(t) - T_{C(2i-1),0}) + \\ + \frac{1}{2}D_{Ci} \cdot (T_{C(2i)}(t) - T_{C(2i),0})] \tag{17}$$

Let us notice that the power distribution coefficients D_{Ci} in Equations (14)-(17) play the role of weight factors. The index '0' denotes the initial values of the fuel and coolant node temperatures.

4.2. Power distribution coefficients

4.2.1. Type I

The first type of power distribution coefficients D_{Ci} considered in the paper is based on the most basic hypothetical assumption that the power generated in the reactor core is uniform and equally distributed along the core height (Naghedolfeizi, 1990). In that case, the values of the thermal power distribution

coefficients D_{Ci} in the expanded multi-node model for each $i-th$ fuel node can be calculated as follows

$$D_{Ci} = \frac{1}{\eta} \qquad for \qquad i = 1, ..., \eta \tag{18}$$

with the assumption that

$$\sum_{i=1}^{\eta} D_{Ci} = 1. \tag{19}$$

For example, in the multi-nodal model with three fuel nodes ($\eta = 3$) all coefficients are equal to 1/3, while in the model with five fuel nodes ($\eta = 5$) they are equal to 1/5, and so on.

4.2.2. Type II

For the second type of power distribution coefficients D_{Ci} proposed by the authors, an assumption is made that the reactor core has cylindrical geometry, as presented in Fig. 6A. Consequently, the values of particular power distribution coefficients D_{Ci} are constant in time and only related to the nominal axial distribution of the neutron flux in the reactor core, that is when control rod bank is fully withdrawn from the reactor core (Fig. 6A).

The axial distribution of the neutron flux in the finite cylindrical volume of the reactor core is approximated using the diffusion equation expressed in terms of the axial coordinate z. For the unrodded reactor region (marked with

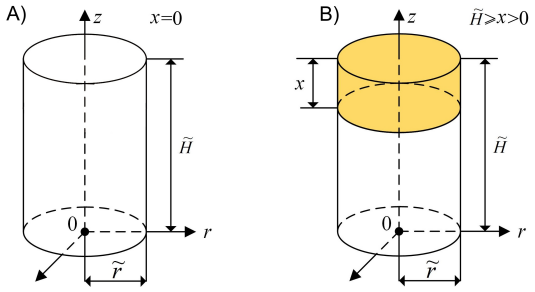

Figure 6: Cylindrical reactor core: A) with the control rod bank withdrawn from reactor, B) with the control rod bank inserted into the reactor to depth x from the top.

subscript u) this equation has the following form (Lewis, 2008)

$$\frac{d^2}{dz^2}\chi_u + \alpha^2\chi_u = 0, \quad 0 \leq z \leq \tilde{H}, \tag{20}$$

where α is defined as (Lewis, 2008)

$$\alpha^2 = \frac{1}{M^2}\left(\frac{k_\infty}{k} - 1\right) - B_r^2, \tag{21}$$

and χ_u is the neutron flux distribution along the z coordinate in the unrodded core, M is the migration length, k_∞ is the infinite multiplication factor, B_r is the radial buckling, and k is the multiplication factor. The solution of the second order ordinary differential equation (20) with the boundary condition $\chi_u(0) = 0$ is given as a function of the axial coordinate z (Lewis, 2008)

$$\chi_u(z) = C\sin(\alpha z), \tag{22}$$

where C is related to the maximum value of the neutron flux χ_u.

Figure 7 shows an appropriate graph of the function $\chi_u(z)$. It has been drawn for the axial neutron flux distribution of the PWR reactor core without the control rod bank (the control rod bank immersion depth $x = 0\%$), assuming that the C parameter (Eq. (22)) was equal 1. Next, the constant power distribution coefficient D_{Ci} is determined for each i-th fuel node. The number of coefficients is strictly related to the number of the considered fuel nodes η. To determine the value of each coefficient, firstly the reactor height is divided into minor intervals for which the coefficient values are calculated. The length of each interval $\Delta\tilde{H} = \tilde{H}/\eta$ is the same and related to the number of fuel nodes η. Next, the limits for each interval are calculated, i.e. the values $h_0, h_1, h_2, ..., h_\eta$ are identified. Then, for each minor interval an area under the neutron flux distribution described by function (22) and limited by particular interval limits is calculated. Finally, each minor area is divided by the total area under the neutron flux distribution function. A precise formula to calculate each D_{Ci} coefficient is given as

$$D_{Ci} = \frac{\int_{h_{i-1}}^{h_i}\chi_u(z)dz}{\int_0^{\tilde{H}}\chi_u(z)dz} \quad \text{for} \quad i = 1, ..., \eta. \tag{23}$$

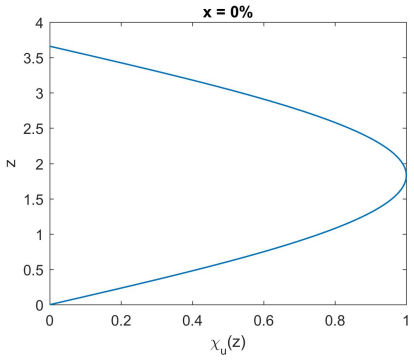

Figure 7: Neutron flux distribution in the cylindrical reactor core with the control rod bank fully withdrawn.

The values of the D_{Ci} coefficients of Type II are listed in Table 1, for 3, 5 and 10 fuel nodes of the considered PWR reactor core, while their graphical representation is shown in Fig. 8.

It can be clearly seen that the D_{ci} coefficients of Type II have values strictly related to the axial distribution of the neutron flux along the reactor core height and symmetrical with respect to the core half-height.

Table 1: D_{ci} coefficients of Type II for the expanded multi-nodal model of PWR reactor core.

i	$D_{ci},\ \eta = 3$	$D_{ci},\ \eta = 5$	$D_{ci},\ \eta = 10$
10	–	–	0.024
9	–	–	0.071
8	–	–	0.110
7	–	–	0.139
6	–	–	0.154
5	–	0.095	0.154
4	–	0.250	0.139
3	0.250	0.309	0.110
2	0.500	0.250	0.071
1	0.250	0.095	0.024

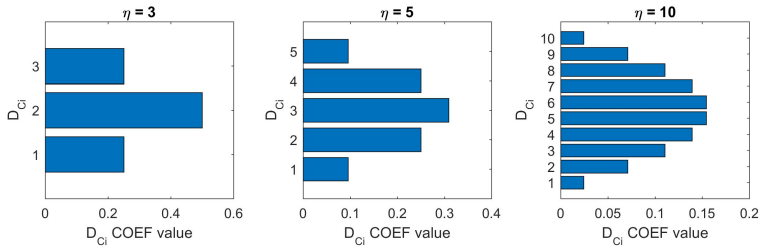

Figure 8: D_{ci} coefficients of Type II for the expanded multi-nodal model of PWR reactor core - with 3, 5 and 10 fuel nodes.

4.2.3. Type III

The third type of power distribution coefficients D_{Ci} proposed by the authors also refers to cylindrical geometry of the reactor core and represents the situation when the power distribution in the core is related to the depth x of control rod bank insertion into the reactor, measured from the top (Fig. 6B). The axial distribution of the neutron flux within the reactor core is also approximated based on the diffusion equation expressed in terms of the axial coordinate z, which in this case takes two forms related to the unrodded (index u) and rodded (index r) reactor regions (Lewis, 2008). Taking into account the insertion depth x, these equations are presented as (Lewis, 2008)

$$\frac{d^2}{dz^2}\chi_u + \alpha^2\chi_u = 0, \quad 0 \le z \le \tilde{H} - x, \tag{24}$$

$$\frac{d^2}{dz^2}\chi_r + \left(\alpha^2 - \beta^2\right)\chi_r = 0, \quad \tilde{H} - x \le z \le \tilde{H}, \tag{25}$$

where the parameter β is defined as (Lewis, 2008)

$$\beta^2 = \frac{1}{M^2}\frac{k_\infty}{k}\rho_b, \tag{26}$$

and χ_r is the neutron distribution along the z coordinates in the rodded part of the reactor core, while ρ_b is the reactivity worth of the bank when it is inserted to the entire length. Here, an assumption is made that the diffusion coefficients in the rodded r and unrodded u core regions are the same (Lewis, 2008).

The solutions of the second order differential equations (24)-(25) are presented in the following forms (Lewis, 2008)

$$\chi_u(z) = C\sin(\alpha z), \tag{27}$$

$$\chi_r(z) = \begin{cases} C'\sin\left[\sqrt{\alpha^2-\beta^2}\left(\tilde{H}-z\right)\right] & \text{if } \alpha^2 > \beta^2, \\ C'\sinh\left[\sqrt{\beta^2-\alpha^2}\left(\tilde{H}-z\right)\right] & \text{if } \alpha^2 < \beta^2, \\ -C'(\tilde{H}-z),\ \alpha^2=\beta^2 & \text{if } \alpha^2 = \beta^2. \end{cases} \tag{28}$$

The C and C' parameters are directly related to each other. The solutions presented by Equations (27)-(28) should fulfil the boundary conditions for the considered reactor design (Lewis, 2008)

$$\chi_u(0) = 0 \quad \text{and} \quad \chi_r\left(\tilde{H}\right) = 0. \tag{29}$$

Moreover, the functions (27)-(28) should have smooth and continuous transition. This condition is presented in the following form Lewis (2008)

$$\chi_u\left(\tilde{H}-x\right) = \chi_r\left(\tilde{H}-x\right), \tag{30}$$

$$\left.\frac{d}{dz}\chi_u(z)\right|_{\tilde{H}-x} = \left.\frac{d}{dz}\chi_r(z)\right|_{\tilde{H}-x}. \tag{31}$$

Applying of the interface conditions (30)-(31) to Equations (27)-(28), leads to additional equations relating C and C'. Taking their ratio C/C' into consideration leads to three additional transcendental equations Lewis (2008)

$$\alpha\cot\left[\alpha\left(\tilde{H}-x\right)\right] = -\sqrt{\alpha^2-\beta^2}\ \cot\left(\sqrt{\alpha^2-\beta^2}x\right) \text{ if } \alpha^2 > \beta^2, \tag{32}$$

$$\alpha\cot\left[\alpha\left(\tilde{H}-x\right)\right] = -\sqrt{\beta^2-\alpha^2}\ \coth\left(\sqrt{\beta^2-\alpha^2}x\right) \text{ if } \alpha^2 < \beta^2, \tag{33}$$

$$-\alpha x = \tan(\alpha(\tilde{H}-x)) \text{ if } \alpha^2 = \beta^2. \tag{34}$$

These transcendental equations (32)-(34) are solved for the unknown variable k, which is also present in Equations (21) and (26). In order to solve these

equations, symbolic and numerical methods were used. The obtained numerical results reveal that Equations (32)-(34) have many solutions over the area of interest specified by the below described limits k_u and k_r

$$k_u = \frac{k_\infty}{1 + M^2(B_r^2 + B_z^2)}, \tag{35}$$

$$k_r = (1 - \rho_b)k_u. \tag{36}$$

The proper solution should not contain discontinuities over that area. In order to select the proper solutions, the authors solved Equations (32)-(34) for 201 linearly spaced points between k_u and k_r, with step $\Delta x = 0.0183$ and discarded those which did not form a continuous set of k values. The solutions selected by the authors are shown in Fig. 9, as an unknown nonlinear function $k = f(x)$ which takes into account the relation between the multiplication coefficient k and the control rod bank immersion depth x. The value of the multiplication factor k_{kr} also shown in Fig. 9) was derived from the relation $\alpha^2 = \beta^2$. Then, for given k_{kr}, the appropriate value of x_{kr} was derived from Equation (34). The values of x_{kr} and k_{kr} are needed to determine the intervals within witch Equations (32) and (33) are valid.

When the control rod bank is inserted into the reactor core to the distance x, the spatial distribution of neutrons within the reactor core is determined from Equations (27)-(28). The constants C and C' in these equations are strictly related to each other and determine the amplitude of the functions that describe the neutron flux distribution within the reactor core. The values of these constants can be derived after applying the interface conditions described by Equations (30)-(31) to Equations (27)-(28). In the presently analysed case the resulting homogeneous system of Equations (30)-(31), should be solved for C and C' with given k. The authors chose the constants C and C' which fulfilled the above mentioned homogeneous system in such a way that for each given immersion depth x the maximum value of the neutron flux was normalized and made equal to one. It should be noted that the selection of these constants

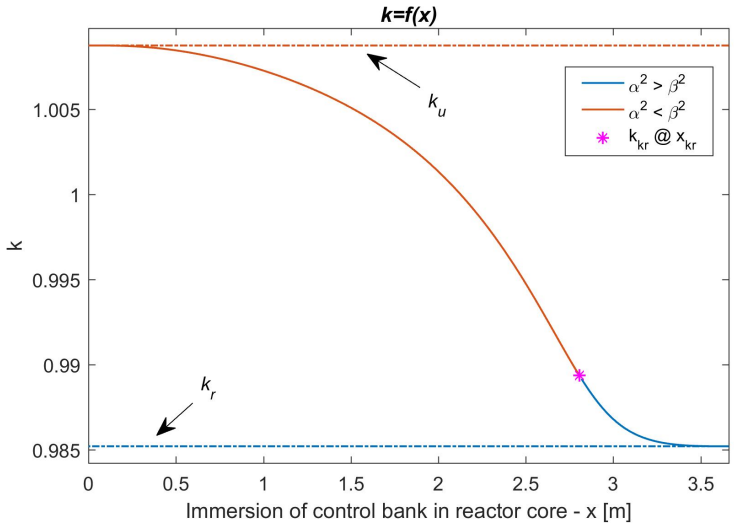

Figure 9: Multiplication coefficient k vs. control rod bank immersion depth into the reactor core x

does not affect the values of the distribution coefficients as long as the interface conditions (30) and (31) are met.

The neutron flux distributions for different depths of control rod bank insertion into the considered PWR reactor core are presented in Fig. 10. Next, based on the information on the number of fuel nodes η, the particular distribution coefficients D_{Ci} corresponding to the current control rod bank insertion depth x were determined. These calculations based on similar assumptions to those stated in subsection 4.2.2. The formula for D_{Ci} coefficients of Type III is analogical to Equation (23) with two exceptions. Firstly, the denominator in formula (23) is to be changed to

$$\int_0^{\tilde{H}-x} \chi_u(z)dz + \int_{\tilde{H}-x}^{\tilde{H}} \chi_r(z)dz \tag{37}$$

to take into account two functions describing the neutron flux distribution. Secondly, one of the intervals limited by h_{i-1} and h_i values for which the coefficients D_{Ci} coefficients are calculated will contain the transition point between the functions, namely $\chi_u(\tilde{H}-x) = \chi_r(\tilde{H}-x)$. In that case one coefficient is to

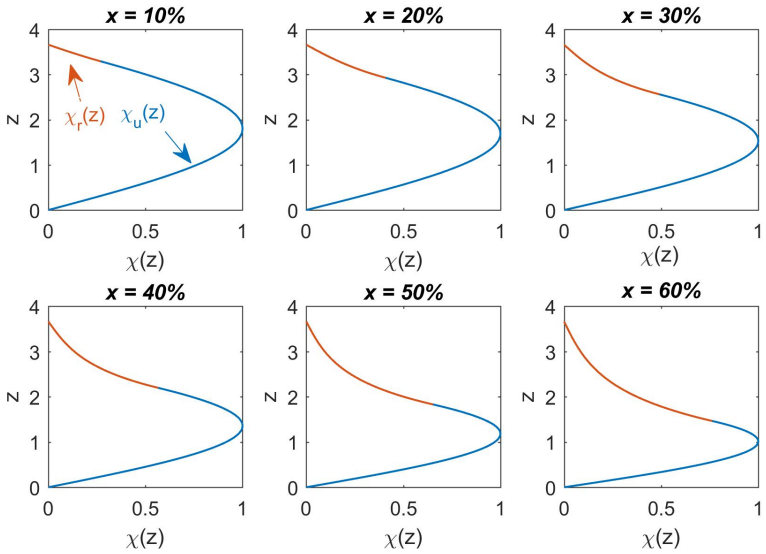

Figure 10: Spatial neutron flux distributions for different control rod bank insertion depths x.

be calculated according to the following formula

$$D_{Ci} = \frac{\int_a^{\tilde{H}-x} \chi_u(z)dz + \int_{\tilde{H}-x}^b \chi_r(z)dz}{\int_0^{\tilde{H}-x} \chi_u(z)dz + \int_{\tilde{H}-x}^{\tilde{H}} \chi_r(z)dz} \tag{38}$$

where the constants a and b are related to the limits of the interval that contains the point $\tilde{H} - x$.

For comparison studies, the authors performed calculations of D_{Ci} coefficients for different numbers of fuel nodes: $\eta = 3$, $\eta = 5$, $\eta = 10$ and for various depths x of control rod bank immersion into the reactor core, expressed in meters and % of reactor core height. The results of these calculations are presented in Tables 2-4 and in Figs. 11-13. It can be clearly seen, that the numerical values of D_{Ci} coefficients are strictly related to power distributions corresponding to control rod bank movements.

Changes of D_{Ci} coefficients may be approximated, according to the control rod bank immersion depth x, by appropriate polynomials with parameters identified using the least squares algorithm. For example, for $\eta = 5$ the approximation of D_{Ci} coefficients may be expressed in the form of fourth degree

Table 2: D_{Ci} coefficients calculated for $\eta = 3$ fuel nodes.

Depth x [m]	0,0000	0,3660	0,7320	1,0980	1,4640	1,8300	2,1960
Depth x [%]	0	10	20	30	40	50	60
D_{C1}	0,2500	0,2562	0,2834	0,3290	0,3904	0,4646	0,5370
D_{C2}	0,5000	0,5055	0,5234	0,5354	0,5170	0,4647	0,3974
D_{C3}	0,2500	0,2383	0,1932	0,1355	0,0926	0,0707	0,0656

Table 3: D_{Ci} coefficients calculated for $\eta = 5$ fuel nodes.

Depth x [m]	0,0000	0,3660	0,7320	1,0980	1,4640	1,8300	2,1960
Depth x [%]	0	10	20	30	40	50	60
D_{C1}	0,0955	0,0981	0,1094	0,1290	0,1567	0,1933	0,2361
D_{C2}	0,2500	0,2556	0,2794	0,3175	0,3642	0,4110	0,4345
D_{C3}	0,3090	0,3127	0,3251	0,3352	0,3258	0,2810	0,2261
D_{C4}	0,2500	0,2468	0,2261	0,1794	0,1262	0,0934	0,0826
D_{C5}	0,0955	0,0868	0,0599	0,0389	0,0270	0,0213	0,0207

Table 4: D_{Ci} coefficients calculated for $\eta = 10$ fuel nodes

Depth x [m]	0,0000	0,3660	0,7320	1,0980	1,4640	1,8300	2,1960
Depth x [%]	0	10	20	30	40	50	60
D_{C1}	0.0245	0.0251	0.0281	0.0334	0.0410	0.0513	0.0641
D_{C2}	0.0710	0.0729	0.0812	0.0956	0.1157	0.1420	0.1720
D_{C3}	0.1106	0.1133	0.1250	0.1444	0.1700	0.1998	0.2259
D_{C4}	0.1394	0.1423	0.1544	0.1731	0.1943	0.2113	0.2087
D_{C5}	0.1545	0.1569	0.1662	0.1777	0.1842	0.1738	0.1401
D_{C6}	0.1545	0.1558	0.1589	0.1575	0.1416	0.1072	0.0861
D_{C7}	0.1394	0.1389	0.1335	0.1154	0.0827	0.0604	0.0522
D_{C8}	0.1106	0.1080	0.0927	0.0640	0.0435	0.0330	0.0304
D_{C9}	0.0710	0.0662	0.0465	0.0301	0.0209	0.0163	0.0158
D_{C10}	0.0245	0.0206	0.0135	0.0088	0.0062	0.0049	0.0049

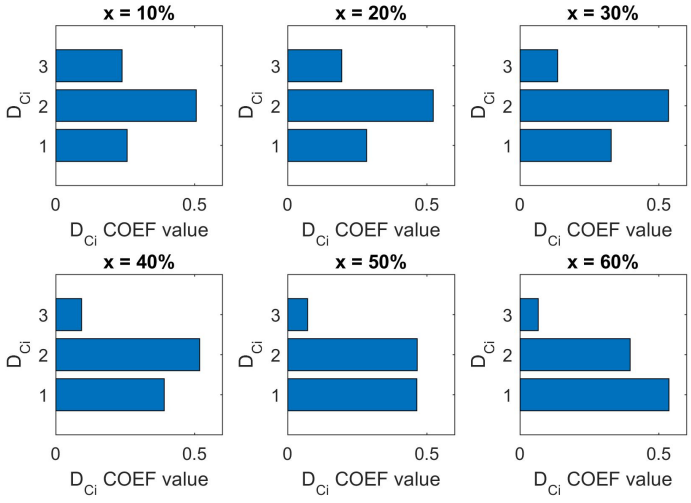

Figure 11: D_{ci} coefficients of type III for different control rod bank insertion depths x and $\eta = 3$ fuel nodes.

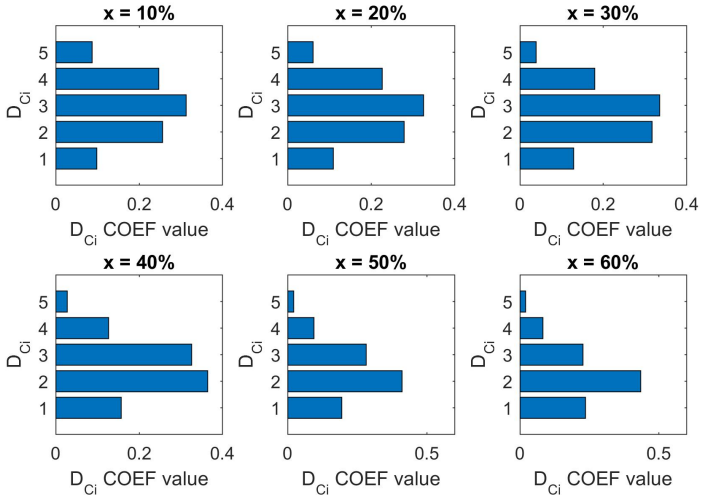

Figure 12: D_{ci} coefficients of type III for different control rod bank insertion depths x and $\eta = 5$ fuel nodes.

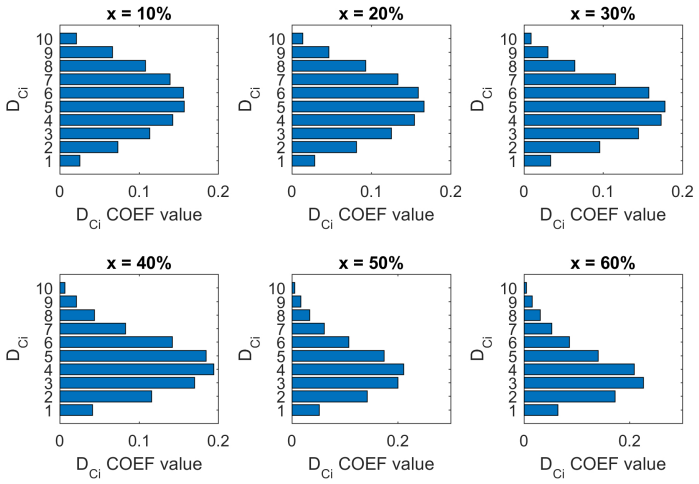

Figure 13: D_{ci} coefficients of type III for different control rod bank insertion depths x and $\eta = 10$ fuel nodes.

polynomials. Let us notice that the power distribution coefficients D_{Ci} are now redefined and expressed as functions $D_{Ci}(x)$ of control rod bank immersion x into the reactor core

$$D_{C1}(x) = -0.00099x^4 + 0.0032x^3 + 0.028x^2 - 0.0033x + 0.095, \tag{39}$$

$$D_{C2}(x) = -0.014x^4 + 0.028x^3 + 0.043x^2 - 0.0016x + 0.25, \tag{40}$$

$$D_{C3}(x) = 0.024x^4 - 0.13x^3 + 0.18x^2 - 0.047x + 0.31, \tag{41}$$

$$D_{C4}(x) = 0.0095x^4 + 0.0072x^3 - 0.11x^2 + 0.04x + 0.25, \tag{42}$$

$$D_{C5}(x) = -0.019x^4 + 0.095x^3 - 0.14x^2 + 0.012x + 0.096. \tag{43}$$

Figure 14 shows the polynomial approximation of the power distribution coefficients $D_{C1}(x)$-$D_{C5}(x)$ described by formulas (39)-(43). Generally, the here described procedure to calculate power distribution parameters gives good results and is proposed to be used within the range 0-60% of the control rod immersion depth x in the reactor core.

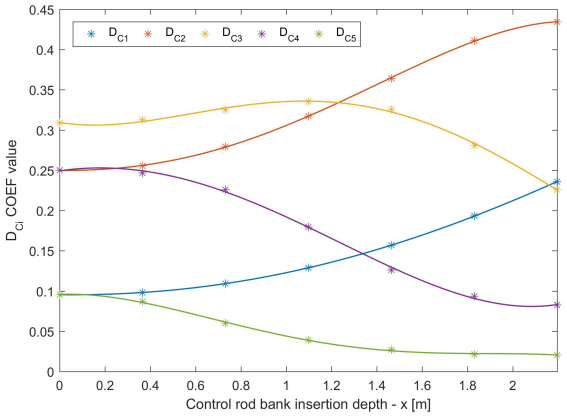

Figure 14: Polynomial approximation of $D_{Ci}(x)$ coefficients for $\eta = 5$.

4.3. Compassion of simulation results obtained using the expanded multi-nodal model

This subsection compares the simulation results obtained using the expanded multi-nodal reactor model. The comparison is made for models consisting of three fuel nodes $\eta = 3$ and five fuel nodes $\eta = 5$, with corresponding six and ten coolant nodes. It mainly focuses on the application of different types of D_{Ci} coefficients in the expanded multi-nodal models presented in the paper (subsections 4.2.1-4.2.3).

The simulation tests were carried out for three different simulation scenarios related to different inputs of the expanded multi-nodal reactor model: (1) the immersion of the control rods, (2) the inlet coolant temperature, and (3) the coolant mass flow rate. These scenarios were changed independently with a negative step from the nominal value of the analysed input variable. In all scenarios the initial position of the control rod bank was set to $x = 30\%$. The variables observed during the simulation included: dynamic changes of the normalized neutron density and the coolant temperature at reactor outlet; the steady state temperatures at all fuel and coolant nodes (the fuel and coolant node temperature profile). Let us notice that each figure (Figs. 15-22) contains four diagrams, of which the diagrams on the left represent dynamic changes of the analysed

variable, while those on the right show its steady-state values. In all diagrams, the labels Type I, Type II and Type III denote the type of the power distribution coefficients $D_{Ci}(x)$ applied to the expanded multi-nodal model. The label 3F/6C is related to the model with three fuel and six coolant nodes, while the label 5F/10C corresponds to the model with five fuel and ten coolant nodes.

Figures 15 and 16 show the responses of the expanded multi-nodal models to a 'small' negative step change of external reactivity, $\Delta\rho = -5$ cents, made at time $t = 5$ second. Similar responses to the step change of negative inlet coolant temperature, $\Delta T_{Cin} = -5\%$ of nominal value, made at the same time $t = 5$ second are shown in Figs. 17 and 18. Figures 19 and 20, in turn, show the responses of the expended multi-nodal models to the step change of negative coolant mass flow rate, $\Delta W_C = -3\%$ of nominal flow, made at $t = 5$ second. Finally, Figs. 21 and 22 present the responses of the expanded multi-nodal models to a 'large' step change of negative external reactivity, to $\Delta\rho = -80$ cents, made at $t = 5$ second.

The figures in this subsection were linked in pairs showing the diagrams for the same simulation scenario but for different numbers of fuel nodes, Figs. 15-16, Figs. 17-18, Figs. 19-20 and Figs. 21-22. When analysing these pairs of figures we can see that dynamic changes of the normalized neutron density and the coolant temperature at reactor outlet are similar in transient conditions and in the steady state. As far as the number of fuel nodes is concerned, it is clearly shown that a greater number of fuel nodes provides better quantitative information about the reactor core temperature profile. Large differences between various types of power distribution coefficients were observed when analysing the fuel and coolant node temperatures. As a result, different temperature profiles were obtained.

When analysing the steady-state temperature of fuel nodes in Figs. 15-22, it can be observed that all fuel nodes have approximately the same temperature values for coefficients of Type I, while for Type II coefficients the fuel nodes have symmetrical temperature values with respect to the half-height of the reactor core. Finally, for Type III coefficients, the temperature profile is asymmetrical

(lower values at the top and higher at the bottom of the reactor core), which reflects the presence of the rodded and unrodded parts of the reactor core. Thus, the third type of power distribution coefficients allows the analysis of reactor core temperature profile changes resulting from control rod bank movements.

bottom to top of the reactor core. In the case of power distribution coefficients of Type I, the coolant nodes temperature increase linearly, while for power coefficients of Type II and Type III their increase is nonlinear. In the case of power distribution coefficient of Type III, the coolant nodes located above the half-height of the reactor have the highest temperatures of all cases and simulation scenarios.

Figures 21-22 show the responses of the expanded multi-nodal models to a 'large' negative step change of external reactivity. Comparing Figs. 15-16 and Figs. 21-22 we can analyse direct impact of the control rod bank immersion depth x on the temperature profile and power distribution coefficients $D_{Ci}(x)$.

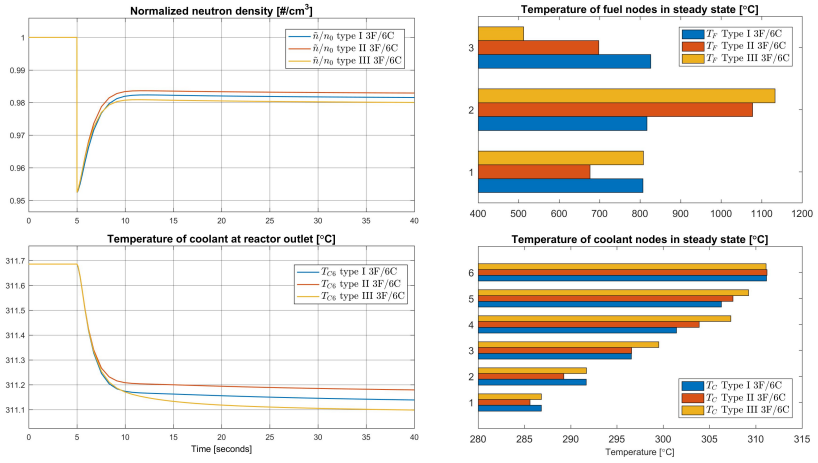

Figure 15: Comparison of models with three fuel nodes – negative reactivity step $\Delta\rho = -5c$.

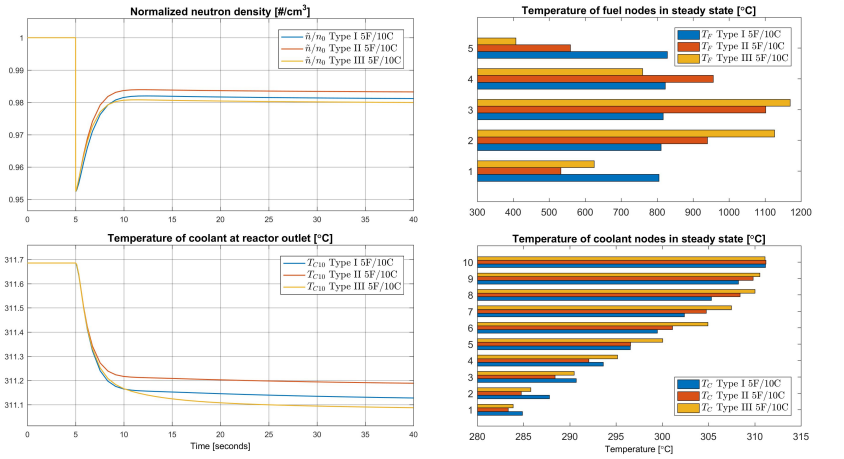

Figure 16: Comparison of models with five fuel nodes – negative reactivity step change $\Delta\rho = -5c$.

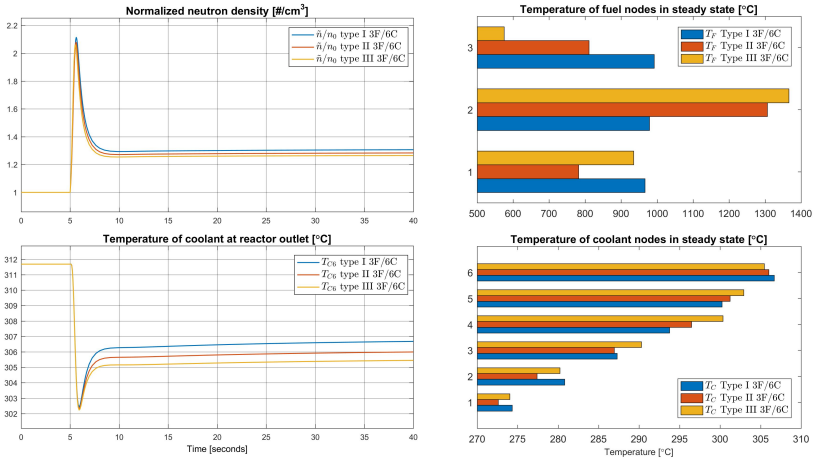

Figure 17: Comparison of models with three fuel nodes – negative temperature step change $\Delta T_{Cin} = -5\%$.

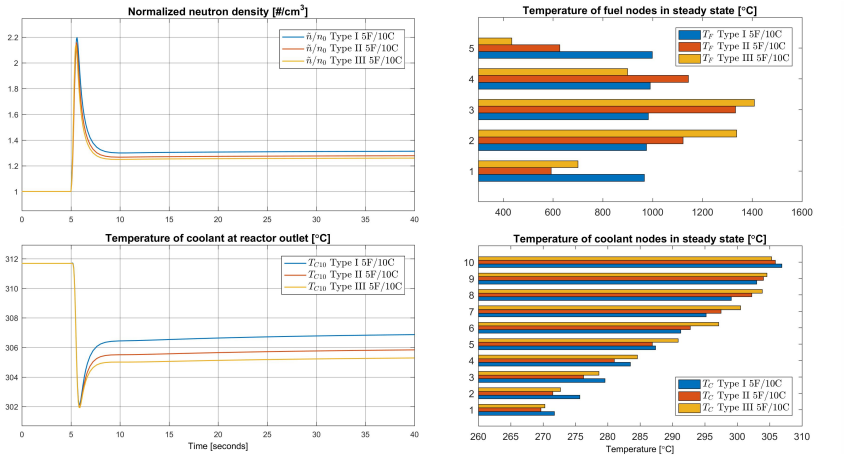

Figure 18: Comparison of models with five fuel nodes – negative temperature step change $\Delta T_{Cin} = -5\%$.

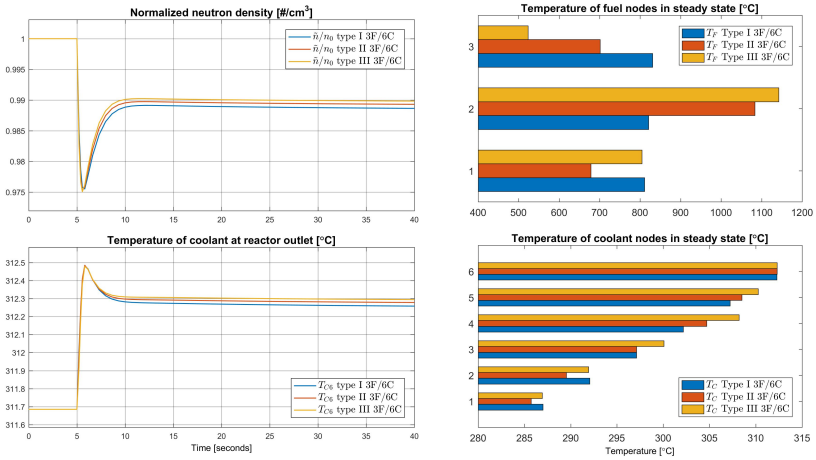

Figure 19: Comparison of models with three fuel nodes – negative mass flow rate step change $\Delta W_C = -3\%$.

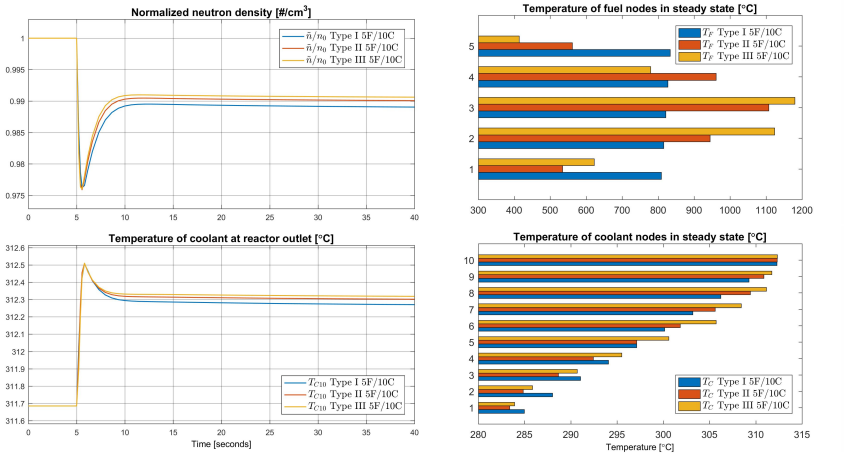

Figure 20: Comparison of models with five fuel nodes – negative mass flow rate step change $\Delta W_C = -3\%$.

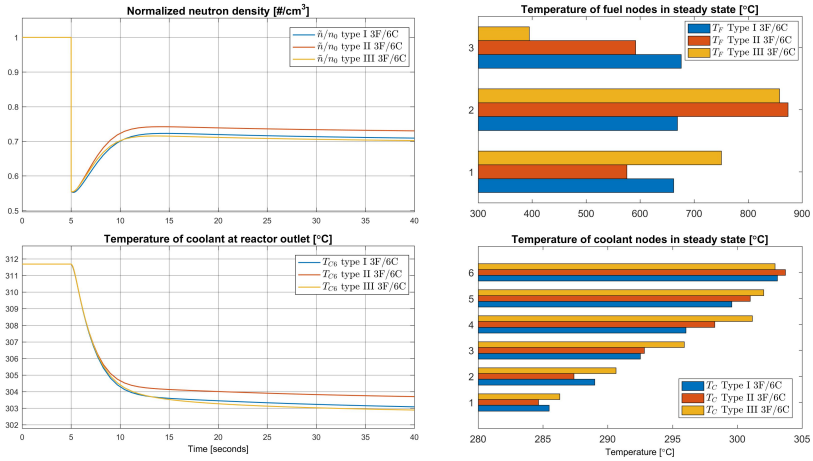

Figure 21: Comparison of models with three fuel nodes – negative reactivity step change $\Delta\rho = -80c$.

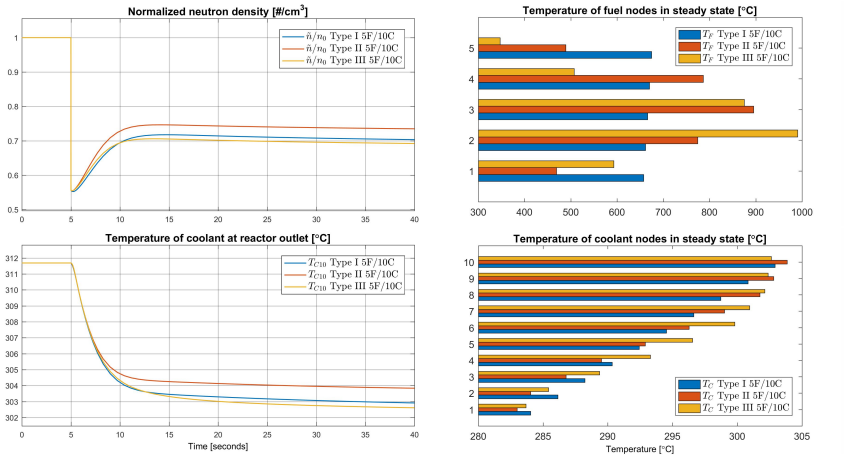

Figure 22: Comparison of models with five fuel nodes – negative reactivity step change $\Delta\rho = -80c$.

Different power distribution coefficient profiles (Type I, Type II, or Type III) lead to different average neutron density and temperature profiles observed at fuel and coolant nodes along the reactor height (Figs. 15-16 and Figs. 21-22, respectively). As for the average thermal power generated at fuel nodes, it is quite similar for the considered models when the power distribution coefficients of Type I and Type III are used. For the Type II coefficients, the average thermal power generated at fuel nodes is larger than that for the two other types. This is the reason why on the diagrams presented in Figs. 15-16 and Figs. 21-22, the trends of coolant temperatures at reactor outlet calculated using Type II coefficients are above the corresponding trends calculated using Type I and Type III coefficients.

4.4. Comparison with dedicated nuclear simulation and analysis software

In the paper, the simulation results obtained using the expanded multi-nodal model were compared also with the default 1D nuclear reactor model implemented in the Apros Nuclear Software (Fortum and VTT, 2017). Parameters from Apros software were recalculated and implemented in the expanded multi-nodal model. Apros Nuclear simulation and analysis software has been

successfully used in a series of major nuclear power plant projects, including power upgrade, modernization, safety improvement, and new plant projects (Fortum and VTT, 2017).

The Apros 1D nuclear reactor model assumes that for each fuel node only one coolant node is used. In this situation, the authors have performed two additional simulations which enabled direct comparison of temperatures at particular fuel and coolant nodes: for five fuel nodes and five coolant nodes (5F/5C), and for ten fuel nodes and ten coolant nodes (10F/10C), respectively. The simulation tests were carried out for the simulation scenario related to the negative step change of external reactivity, $\Delta\rho = -80c$, made at time $t = 5$ second (initial position of the control rod bank was set to $x = 0\%$). The variables observed during the simulation included: dynamic changes of normalized neutron density and coolant temperature at reactor outlet (Figs. 23- 24), and steady-state temperatures at all fuel and coolant nodes, considered as the fuel and coolant node temperature profile (Fig. 25).

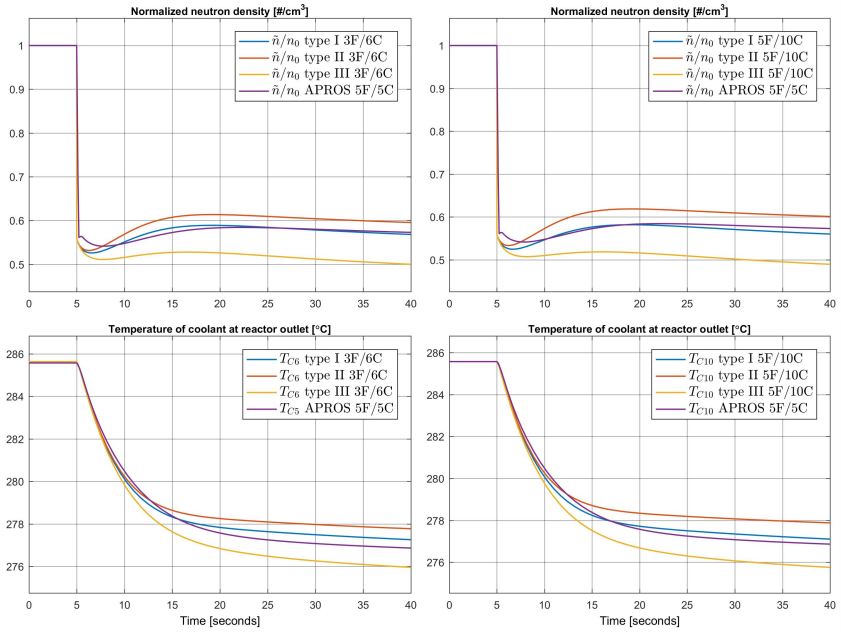

Figure 23: Comparing the Apros 1D nuclear reactor model (5F/5C), and the expanded multi-nodal reactor model with various power distribution coefficients and model structure.

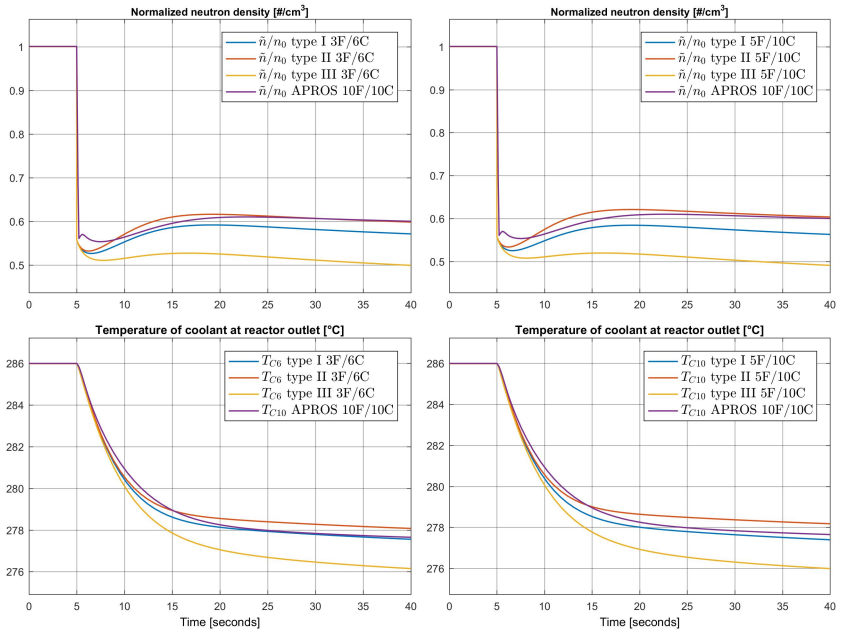

Figure 24: Comparing the Apros 1D nuclear reactor model (10F/10C), and the expanded multi-nodal reactor model with various power distribution coefficients and model structure.

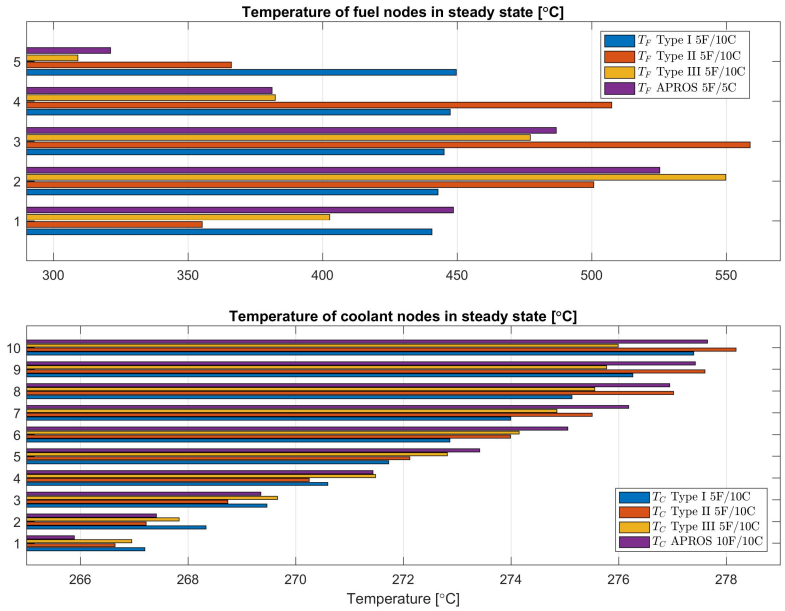

Figure 25: Comparing the Apros 1D nuclear reactor model and the expanded multi-nodal reactor models with various coefficients and structures: steady-state temperatures.

When analysing the results presented in Fig. 23 and Fig. 24, can be seen that dynamic changes of normalized neutron densities and coolant temperatures at reactor outlet are quite similar in transient conditions and in the steady states. It is clearly seen that the expanded multi-nodal model with power distribution coefficients of Type I has the closest fit to the Apros 1D nuclear reactor model with 5F/5C node configuration. This closest fit exists for two cases of the analysed expanded multi-nodal model node configurations, namely for cases 3F/6C and 5F/10C. With the increasing number of fuel and coolant nodes in the Apros 1D nuclear reactor model (from five to ten - Fig. 24), the best fit visibly changes to the expanded multi-nodal reactor model with power distribution coefficients of Type II. This situation is observed for the average neutron density in both considered node structures, i.e. cases 3F/6C and 5F/10C. On the other hand, for the coolant temperature at reactor outlet, the simulation results are still quite similar to those obtained using the expanded multi-nodal reactor

model with power distribution coefficients of Type I. The fuel node temperature profile shown in Fig. 25 is highly asymmetrical. This fact clearly indicates that both models have similar functionality related to the approximation of axial thermal power distribution along the reactor core. However, based on the simulation results it can be concluded that, despite certain differences between the compared calculation codes, the obtained simulation results are quite similar and satisfactory. Better fit of the presented results can be achieved by more precise tuning of model parameters or by appropriate identification techniques, but this issue goes beyond the topic of the present paper.

5. Conclusions

The commonly known multi-nodal model of reactor core was expanded using thermal power distribution coefficients D_{Ci}, to introduce thermal power distribution functionality to the model. The comparison of simulation results for nodal and multi-nodal models was carried out. The research has showed that introduction of power distribution coefficients into nodal model of nuclear reactor core can increase its usefulness. The main advantage of the expanded multi-nodal model approach is that the temperatures in different zones of the reactor core may be efficiently and more precisely estimated. This approach can lead to the development of more advanced control systems for reactor cores, which can take into account different fuel and coolant temperatures. Introducing thermal power distribution coefficients makes it also possible to calculate not only temperatures in different parts of the reactor, but also thermal power distribution changes. These data can be useful in various analyses performed for control system synthesis purposes.

Appendix A. Parameters and initial conditions

Table A.5: Parameters of the nuclear reactor core models. Nominal parameters for 100% power output are marked with index N.

β		0.0065	Λ	s	0.0000179	m_F	kg	101032.71
β_1		0.000215	λ_1		0.0124	m_C	kg	11196.20
β_2		0.001424	λ_2		0.0305	c_{pF}	$\frac{J}{kg\,^\circ C}$	247.02
β_3	–	0.001274	λ_3	$\frac{1}{s}$	0.1110	c_{pC}	$\frac{J}{kg\,^\circ C}$	5819.65
β_4		0.002568	λ_4		0.3010	f_F	–	0.974
β_5		0.000748	λ_5		1.1400	A	m^2	5564.89
β_6		0.000273	λ_6		3.0100	h	$\frac{W}{m^2\,^\circ C}$	1135.65
α_F	$\frac{1}{^\circ C}$	-1.98×10^{-5}	α_C	$\frac{1}{^\circ C}$	-3.6×10^{-5}	$N_{0,N}$	$\frac{n}{cm^3}$	249952819.52
$P_{TH,N}$	MW	3436	$W_{C,N}$	$\frac{kg}{s}$	19851.92	$T_{C,in,N}$	$^\circ C$	281.94

Table A.6: Initial conditions for nodal model 1F/1C and 1F/2C.

$C_{1,0}$		2.4212	$T_{F1,0}^{1F/1C}$		826.3684
$C_{2,0}$		6.5195	$T_{C1,0}^{1F/1C}$		296.8149
$C_{3,0}$	$\frac{n}{cm^3} * 10^{11}$	1.6027	$T_{F1,0}^{1F/2C}$	$^\circ C$	826.3684
$C_{4,0}$		1.1913	$T_{C1,0}^{1F/2C}$		296.8149
$C_{5,0}$		0.0916	$T_{C2,0}^{1F/2C}$		311.6853
$C_{6,0}$		0.0127			

Table A.7: Fuel and coolant nodes temperature initial conditions for model 3F/6C with respect to type I,II,III D_{Ci} coefficients.

$T^{I}_{F1,0}$		816.4547	$T^{I}_{C1,0}$		286.9013	$T^{II}_{C4,0}$		304.2501
$T^{I}_{F2,0}$		826.3684	$T^{I}_{C2,0}$		291.8581	$T^{II}_{C5,0}$		307.9677
$T^{I}_{F3,0}$		836.2820	$T^{I}_{C3,0}$		296.8149	$T^{II}_{C6,0}$		311.6853
$T^{II}_{F1,0}$		682.8272	$T^{I}_{C4,0}$		301.7717	$T^{III}_{C1,0}$		286.8368
$T^{II}_{F2,0}$	$^{\circ}C$	1091.1451	$T^{I}_{C5,0}$	$^{\circ}C$	306.7285	$T^{III}_{C2,0}$	$^{\circ}C$	291.7293
$T^{II}_{F3,0}$		705.1328	$T^{I}_{C6,0}$		311.6853	$T^{III}_{C3,0}$		299.6916
$T^{III}_{F1,0}$		809.5095	$T^{II}_{C1,0}$		285.6621	$T^{III}_{C4,0}$		307.6540
$T^{III}_{F2,0}$		1150.3394	$T^{II}_{C2,0}$		289.3797	$T^{III}_{C5,0}$		309.6696
$T^{III}_{F3,0}$		525.0097	$T^{II}_{C3,0}$		296.8149	$T^{III}_{C6,0}$		311.6853

Table A.8: Fuel nodes temperature initial conditions for model 5F/10C with respect to type I,II,III D_{Ci} coefficients.

$T^{I}_{F1,0}$		814.4720	$T^{II}_{F1,0}$		536.2037	$T^{III}_{F1,0}$		625.3150
$T^{I}_{F2,0}$		820.4202	$T^{II}_{F2,0}$		950.4439	$T^{III}_{F2,0}$		1131.1650
$T^{I}_{F3,0}$	$^{\circ}C$	826.3684	$T^{II}_{F3,0}$	$^{\circ}C$	1115.0200	$T^{III}_{F3,0}$	$^{\circ}C$	1187.8225
$T^{I}_{F4,0}$		832.3165	$T^{II}_{F4,0}$		967.0696	$T^{III}_{F4,0}$		782.9781
$T^{I}_{F5,0}$		838.2647	$T^{II}_{F5,0}$		563.1046	$T^{III}_{F5,0}$		414.0259

Table A.9: Coolant nodes temperature initial conditions for model 5F/10C with respect to type I,II,III D_{Ci} coefficients.

$T^{I}_{C1,0}$		284.9185	$T^{II}_{C1,0}$		283.3644	$T^{III}_{C1,0}$		283.8621
$T^{I}_{C2,0}$		287.8926	$T^{II}_{C2,0}$		284.7844	$T^{III}_{C2,0}$		285.7798
$T^{I}_{C3,0}$		290.8667	$T^{II}_{C3,0}$		288.5021	$T^{III}_{C3,0}$		290.5011
$T^{I}_{C4,0}$		293.8408	$T^{II}_{C4,0}$		292.2197	$T^{III}_{C4,0}$		295.2225
$T^{I}_{C5,0}$	$^{\circ}C$	296.8149	$T^{II}_{C5,0}$	$^{\circ}C$	296.8149	$T^{III}_{C5,0}$	$^{\circ}C$	300.2075
$T^{I}_{C6,0}$		299.789	$T^{II}_{C6,0}$		301.4101	$T^{III}_{C6,0}$		305.1926
$T^{I}_{C7,0}$		302.763	$T^{II}_{C7,0}$		305.1277	$T^{III}_{C7,0}$		307.8609
$T^{I}_{C8,0}$		305.7371	$T^{II}_{C8,0}$		308.8453	$T^{III}_{C8,0}$		310.5293
$T^{I}_{C9,0}$		308.7112	$T^{II}_{C9,0}$		310.2653	$T^{III}_{C9,0}$		311.1073
$T^{I}_{C10,0}$		311.6853	$T^{II}_{C10,0}$		311.6853	$T^{III}_{C10,0}$		311.6853

Table A.10: Additional parameters used in calculations of D_{Ci} coefficients.

M	m	0.0762	B_z	1/m	0.8584
k_∞	–	1.0250	ρ_b	–	0.0233
B_r	1/m	1.4273	$\tilde{H}$	m	3.6600

References

Dong, Z., Huang, X., Feng, J., Zhang, L., 2009. Dynamic model for control system design and simulation of a low temperature nuclear reactor. Nuclear Engineering and Design 239, 2141–2151. doi:10.1016/j.nucengdes.2009.05.006.

Dong, Z., Huang, X., Zhang, L., 2010. A nodal dynamic model for control system design and simulation of an MHTGR core. Nuclear Engineering and Design 240, 1251–1261. doi:10.1016/j.nucengdes.2009.12.032.

Duderstadt, J.J., Hamilton, L.J., 1976. Nuclear reactor analysis. Wiley.

Espinosa-Paredes, G., Polo-Labarrios, M.A., Espinosa-Martínez, E.G., Valle-Gallegos, E.d., 2011. Fractional neutron point kinetics equations for nuclear reactor dynamics. Annals of Nuclear Energy 38, 307–330. doi:10.1016/j.anucene.2010.10.012.

Fazekas, C., Szederkényi, G., Hangos, K., 2007. A simple dynamic model of the primary circuit in VVER plants for controller design purposes. Nuclear Engineering and Design 237, 1071–1087. doi:10.1016/j.nucengdes.2006.12.002.

Fortum, VTT, 2017. Apros - Dynamic Process Simulation Software for Nuclear and Thermal Power Plant Applications. URL: http://www.apros.fi/en.

Guimarães, L.N.F., Oliveira, N.d.S., Borges, E.M., 2008. Derivation of a nine variable model of a U-tube steam generator coupled with a three-element controller. Applied Mathematical Modelling 32, 1027–1043. doi:10.1016/j.apm.2007.02.022.

Han, G.Y., 2000. A mathematical model for the thermal-hydraulic analysis of nuclear power plants. International Communications in Heat and Mass Transfer 27, 795–805. doi:10.1016/S0735-1933(00)00160-3.

Kapernick, J.R., 2015. Dynamic Modeling of a Small Modular Reactor for Control and Monitoring. Ph.D. thesis. University of Tennessee.

Karla, T., Tarnawski, J., Duzinkiewicz, K., 2015. Cross-platform real-time nuclear reactor basic principle simulator, in: 2015 20th International Conference on Methods and Models in Automation and Robotics (MMAR), IEEE. pp. 1074–1079. doi:10.1109/MMAR.2015.7284028.

Kerlin, T., 1978. Dynamic Analysis and Control of Pressurized Water Reactors, pp. 103–212. doi:10.1016/B978-0-12-012714-6.50008-8.

Kulkowski, K., Kobylarz, A., Grochowski, M., Duzinkiewicz, K., 2015. Dynamic model of nuclear power plant steam turbine. Archives of Control Sciences 25, 65–86. doi:10.1515/acsc-2015-0005.

Lewis, E.E., 2008. Fundamentals of Nuclear Reactor Physics. Elsevier. doi:10.1016/B978-0-12-370631-7.X0001-0.

Liu, X., 2015. Modeling and Simulation of a Prototypical Advanced Reactor. Ph.D. thesis. University of Tennessee.

Naghedolfeizi, M., 1990. Dynamic Modeling of a Pressurized Water Reactor Plant for Diagnostics and Control. Ph.D. thesis. University of Tennessee.

Nowak, T.K., Duzinkiewicz, K., Piotrowski, R., 2014a. Fractional neutron point kinetics equations for nuclear reactor dynamics Numerical solution investigations. Annals of Nuclear Energy 73, 317–329. doi:10.1016/j.anucene.2014.07.001.

Nowak, T.K., Duzinkiewicz, K., Piotrowski, R., 2014b. Numerical Solution of Fractional Neutron Point Kinetics Model in Nuclear Reactor. Archives of Control Sciences 24, 129–154. doi:10.2478/acsc-2014-0009.

Nowak, T.K., Duzinkiewicz, K., Piotrowski, R., 2015. Numerical solution analysis of fractional point kinetics and heat exchange in nuclear reactor. Nuclear Engineering and Design 281, 121–130. doi:10.1016/j.nucengdes.2014.11.028.

Perillo, S.R.P., 2010. Multi-Modular Integral Pressurized Water Reactor Control and Operational Reconfiguration for a Flow Control Loop. Ph.D. thesis. University of Tennessee.

Puchalski, B., Duzinkiewicz, K., Rutkowski, T., 2015a. Multi-region fuzzy logic controller with local PID controllers for U-tube steam generator in nuclear power plant. Archives of Control Sciences 25, 429–444. doi:10.1515/acsc-2015-0028.

Puchalski, B., Rutkowski, T., Tarnawski, J., Duzinkiewicz, K., 2015b. Comparison of tuning procedures based on evolutionary algorithm for multi-region fuzzy-logi PID controller for non-linear plant, in: 2015 20th International

Conference on Methods and Models in Automation and Robotics (MMAR), IEEE. pp. 897–902. doi:10.1109/MMAR.2015.7283996.

Puchalski, B., Rutkowski, T.A., Duzinkiewicz, K., 2016. Multi-nodal PWR reactor model - Methodology proposition for power distribution coefficients calculation, in: 2016 21st International Conference on Methods and Models in Automation and Robotics, MMAR 2016, IEEE. pp. 385–390. doi:10.1109/MMAR.2016.7575166.

Sharma, G., Bandyopadhyay, B., Tiwari, A., 2003. Spatial control of a large pressurized heavy water reactor by fast output sampling technique. IEEE Transactions on Nuclear Science 50, 1740–1751. doi:10.1109/TNS.2003.818271.

Sokolski, P., Rutkowski, T.A., Duzinkiewicz, K., 2016. Simplified, multiregional fuzzy model of a nuclear power plant steam turbine, in: 2016 21st International Conference on Methods and Models in Automation and Robotics (MMAR), IEEE. pp. 379–384. doi:10.1109/MMAR.2016.7575165.

Tarnawski, J., Karla, T., 2016. Real-time simulation in non real-time environment, in: 2016 21st International Conference on Methods and Models in Automation and Robotics (MMAR), IEEE. pp. 577–582. doi:10.1109/MMAR.2016.7575200.

Tiwari, A., Banyopadhyay, B., Govindarajan, G., 1996. Spatial control of a large pressurized heavy water reactor. IEEE Transactions on Nuclear Science 43, 2440–2453. doi:10.1109/23.531794.

Zhang, T., 2012. Comparison of Distributed Parameter and Multi-lump Models for a Pressurized Water Reactor Core. Ph.D. thesis. Arizona State University.

Zhang, T., E. Holbert, K., 2013. Frequency Domain Comparison of Multi-lump and Distributed Parameter Models for Pressurized Water Reactor Cores. American Journal of Energy Research 1, 17–24. doi:10.12691/ajer-1-1-3.